



Corticosteroids reduce pathological angiogenesis yet compromise reparative vascular remodeling in a model of retinopathy

Masayuki Hata^{a,b} , Maki Hata^a, Agnieszka Dejda^a , Frédérique Pilon^a, Roberto Diaz-Marin^b , Frédéric Fournier^a , Jean-Sebastien Joyal^c, Gael Cagnone^c , Yotaro Ochi^d, Sergio Crespo-García^{a,b}, Ariel M. Wilson^a, and Przemyslaw Sapięha^{a,b,1}

Affiliations are included on p. 7.

Edited by Akrit Sodhi, Johns Hopkins University School of Medicine, Baltimore, MD; received June 11, 2024; accepted October 11, 2024 by Editorial Board Member Krzysztof Palczewski

Tissue inflammation is often broadly associated with cellular damage, yet sterile inflammation also plays critical roles in beneficial tissue remodeling. In the central nervous system, this is observed through a predominantly innate immune response in retinal vascular diseases such as age-related macular degeneration, diabetic retinopathy, and retinopathy of prematurity. Here, we set out to elucidate the dynamics of the immune response during progression and regression of pathological neovascularization in retinopathy. In a mouse model of oxygen-induced retinopathy, we report that dexamethasone, a broad-spectrum corticosteroid, suppresses initial formation of pathological preretinal neovascularization in early stages of disease, yet blunts reparative inflammation by impairing distinct myeloid cell populations, and hence reduces beneficial vascular remodeling in later stages of disease. Using genetic depletion of distinct components of the innate immune response, we demonstrate that CX3C chemokine receptor 1-expressing microglia contribute to angiogenesis. Conversely, myeloid cells expressing lysozyme 2 are recruited to sites of damaged blood vessels and pathological neovascularization where they partake in a reparative process that ultimately restores circulatory homeostasis to the retina. Hence, the Janus-faced properties of anti-inflammatory drugs should be considered, particularly in stages associated with persistent neovascularization.

retina | angiogenesis | inflammation | dexamethasone | retinopathy

Retinal homeostasis is reliant on innate immunity (1). Microglia, monocytes, mononuclear phagocytes (MNPs), and neutrophils have been well studied in the sterile inflammatory response during retinal disease (2, 3) where they partake in mediating both seemingly destructive processes such as pathological angiogenesis (4–6) and phagocytosis of damaged photoreceptor cells (7, 8) as well as reparative events such as pruning diseased blood vessels (9, 3). The dual function of the immune response suggests that use of anti-inflammatory strategies must be staged in order to preserve beneficial properties of the immune response while blunting excessive cytokine production in order to ensure retinal homeostasis and proper sight.

Corticosteroid and specifically glucocorticoid drugs are among the most widely used pharmaceutical products in the industrialized world due to their potent immunomodulatory effects (10, 11). The first clinical confirmation for corticosteroids came in the 1930s when animal adrenocortical tissue was shown to improve outcome of adrenal failure in humans (12) and first patients were treated with cortisone for rheumatoid arthritis in 1948 (13). Chemical modifications of the steroid skeleton led to highly potent anti-inflammatory glucocorticoids such as dexamethasone that have been in use since the late 1950s (14). In ophthalmology, corticosteroids are currently widely used for a variety of ophthalmic conditions with local administration for conditions such as conjunctivitis and keratitis, noninfectious posterior uveitis, macular edema due to retinal vasculitis, and diabetic retinopathy and systemic administration for scleritis and optic neuritis (15, 16). Given the broad spectrum of action of corticosteroids, their indication typically implies a lack of clear mechanistic understanding of underlying disease process.

In light of common use of corticosteroids in clinical treatment of prevalent sight-threatening complications such as diabetic macular edema (17, 18), we explored the consequence of intravitreal dexamethasone treatment on tissue remodeling in a mouse model of pathological retinal neovascularization (19). We focused on distinct stages of retinopathy such as pathological neovascularization and beneficial vascular remodeling. Additionally, we investigated the contribution of local CX3CR1⁺ resident immune cells and myeloid-derived lysozyme 2 (LysM)⁺ retinal MNPs in vascular remodeling during retinopathy.

Significance

Retinal vasculopathies such as age-related macular degeneration, diabetic retinopathy, and retinopathy of prematurity are among the leading causes of loss of sight in industrialized countries. While they are associated with heightened inflammation, our study demonstrates that distinct populations of innate immune cells expressing lysozyme 2, can be beneficial and partake in eliminating diseased blood vessels. Our study also highlights that in a mouse model, broad-spectrum anti-inflammatory drugs such as corticosteroids can blunt pathological angiogenesis but also compromise the retina's endogenous repair mechanisms in a disease-stage-specific manner.

Author contributions: Masayuki Hata and P.S. designed research; Masayuki Hata, Maki Hata, A.D., F.P., R.D.-M., F.F., S.C.-G., and A.M.W. performed research; P.S. contributed new reagents/analytic tools; Masayuki Hata, Maki Hata, A.D., J.-S.J., G.C., and Y.O. analyzed data; and Masayuki Hata, A.M.W., and P.S. wrote the paper.

The authors declare no competing interest.

This article is a PNAS Direct Submission A.S. is a guest editor invited by the Editorial Board.

Copyright © 2024 the Author(s). Published by PNAS. This article is distributed under Creative Commons Attribution-NonCommercial-NoDerivatives License 4.0 (CC BY-NC-ND).

¹To whom correspondence may be addressed. Email: mike.sapieha@umontreal.ca.

This article contains supporting information online at <https://www.pnas.org/lookup/suppl/doi:10.1073/pnas.2411640121/-/DCSupplemental>.

Published December 18, 2024.

Results

Dexamethasone Treatment Suppresses Pathological Neovascularization in Early Stages but Prevents Reparative Vascular Remodeling in Later Stages of Disease.

To investigate the effects of anti-inflammatory drugs such as glucocorticoid steroids on pathological vascularization in the retina, we employed the mouse model of oxygen-induced retinopathy (OIR) that is characterized by ischemic retinal tissues and deregulated angiogenesis (19). Mouse pups were exposed to 75% oxygen from postnatal day (P) 7 to P12 to trigger vaso-oblivation, then returned to room air to initiate a second phase of pathological neovascularization that peaks at P17 and is followed by a phase of vascular regression (Fig. 1A). To elucidate general biological processes at play during the progression of retinopathy, we conducted a time-course analysis of transcriptomic changes through bulk-RNA sequencing during distinct stages of OIR (9, 20, 21) at P14 (during neovascularization), P17 (at maximal neovascularization), and P30 (following vascular normalization) and investigated enriched gene sets using Gene Ontology (GO). We observed transcript enrichment in processes related to inflammation/immune response, metabolic process, angiogenesis, and hypoxia at P14 during initiation of preretinal neovascularization, and inflammation/immune response, wound healing, and angiogenesis at P17 of OIR during peak neovascularization (Fig. 1B and *SI Appendix, Fig. S1*). At P30, following vascular normalization, inflammatory genes are regulated, but possibly to a lesser extent, with genes corresponding to “negative regulation of immune system process” appearing to be highly induced (Fig. 1B).

To verify these findings, we investigated individual transcripts by qPCR. We observed induction of *Tnf*, *Il6*, and *Ccl2* throughout the course of pathological neovascularization (P13-P17) and vascular regression (P17-P21) (Fig. 1C–F). *Il1b* was induced around peak neovascularization and persisted (Fig. 1F).

Next, we evaluated the effects of anti-inflammatory treatments on tissue repair, (specifically vascular remodeling) during retinopathy. We injected 0.3 μ g of dexamethasone into the vitreous of C57BL/6J mice at P14, during onset of neovascularization (Fig. 1G). Dexamethasone is a small molecule that is rapidly cleared from the vitreous with an estimated half-life of ~5 to 6 h in human vitreous (22). The swift clearance results in a sharp decline in retinal drug concentrations which allows to draw conclusion on the role of early versus late inflammation in the mouse model of retinopathy.

As expected, at P17, dexamethasone suppressed expression of *Tnf*, *Il6*, *Il1b*, and *Ccl2* as assessed by qPCR (Fig. 1H). Accordingly, dexamethasone-treated eyes had fewer IBA1-expressing phagocytes, both within and outside neovascular tufts (Fig. 1I) measured in retinal flatmounts. Importantly, compared to vehicle controls, treatment of OIR retinas with dexamethasone (DEX) at P14 significantly reduced areas of pathological neovascularization (Fig. 1J) and increased vascular regeneration (Fig. 1K) as assessed at P19.

To investigate the impact of intravitreal dexamethasone on vascular remodeling, we next treated mouse pups at P17 during maximal neovascularization (Fig. 1L). Evaluation of retinas at P19 revealed that dexamethasone led to a nonsignificant trend in decrease of *Tnf*, *Il6*, and *Ccl2* (Fig. 1M) accompanied by a decrease in IBA1-positive inflammatory phagocytes both inside and outside of neovascular tufts (Fig. 1N). In contrast to early treatment with dexamethasone at P14, late administration at P17 significantly compromised regression of pathological neovascularization and slowed vascular regeneration (Fig. 1O and P). Collectively, intravitreal dexamethasone in early stages of neovascularization prevented pathological angiogenesis, yet later administration blunted beneficial vascular remodeling.

Intravitreal Dexamethasone Reduces the Number of Endothelial Cells Undergoing Apoptosis within Pathological Neovascularization.

Pruning of pathological neovascularization requires elimination of endothelial cells through apoptotic mechanisms (9, 3). Using flowcytometry during stages of vascular normalization at P19 OIR, we found increased numbers of Annexin V-positive endothelial cells during regression of pathological blood vessels (*SI Appendix, Fig. S2 A and B*). Consistent with compromised vascular remodeling, retinas from mice treated with dexamethasone at P17 had significantly fewer Annexin V-positive endothelial cells (*SI Appendix, Fig. S2 A and B*). Cleaved caspase 3 staining confirmed that apoptotic cells were primarily confined to sites of pathological neovascularization (tufts) (*SI Appendix, Fig. S2 C and D*) and quantification confirmed that dexamethasone significantly reduced cleaved caspase 3-expressing apoptotic cells within pathological neovascularization. Altogether, these data demonstrate a reduction of endothelial cell apoptosis or compromised clearance of pathological blood vessels secondary to suppression of myeloid cell function as supported by a previous study (9).

Distinct innate Immune Cell Populations Contribute to Neovascularization and Vascular Remodeling of OIR.

Corticosteroids such as dexamethasone have broad immunosuppressive effects, independent of immune cell populations. Consistent with this, flow cytometry analysis showed dexamethasone administration decreased lymphocytes (CD45⁺/CD11b⁻/CD3e⁺), microglia (CD45⁺/CD11b⁺/CX3CR1⁺), and MNP (CD45⁺/CD11b⁺/Ly6C^{int/high}/Ly6G^{low}) in the retina at P17 of OIR (Fig. 2A, with gating in *SI Appendix, Fig. S3*), and microglia, MNP, and neutrophils (CD45⁺/CD11b⁺/Ly6C^{int}/Ly6G^{high}) in the retina at P19 of OIR (Fig. 2B).

To identify potential cell populations associated with clearance of pathological neovascularization from peak neovascularization at P17 of OIR, we performed single-cell RNA sequencing (scRNA-seq). Principal components analysis (PCA) and UMAP plot of different clustered retinal immune cell types with similar transcriptional profiles revealed 8 independent subpopulations present in the retina (Fig. 2C). Marker gene expression analysis identified cluster #1 as Dendritic Cells, #2 as neutrophils, #3-6 as microglia, #7 as macrophages, and #8 as monocytes (*SI Appendix, Fig. S4*). Consistent with qPCR data above (Fig. 1C–F), pathway analysis confirmed increased TNF signaling at P14, whereas IL6 signaling was induced at P17 (Fig. 2D). Notably, cluster #2 (neutrophils) and #3 (microglia) showed the most enrichment in inflammatory pathways at P14, while #2 (neutrophils) and #8 (monocytes) showed the most enrichment in inflammatory processes at P17.

LysM⁺ Monocytes Mediate Vascular Remodeling in Later Stages of OIR while CX3CR1-Expressing Cells Primarily Contributing to Angiogenesis.

scRNA-seq data revealed that monocytes (cluster #8) expressed *Lyz2* but not *Cx3cr1*, while *Cx3cr1* was highly expressed in microglia (cluster #4) and to a lesser extent in monocytes (cluster #8) (Fig. 3A). To assess the contribution of each population of innate immune cells on pathological angiogenesis and vascular remodeling, we generated mice expressing diphtheria toxin (DTx) receptor under control of *Lyz2* or *Cx3cr1* promoters. These mice allow investigation of the contribution of each cell population to vascular phenotypes through selective and time-specific ablation of monocyte-derived LysM-expressing cells or microglia-expressing CX3CR1 secondary to intravitreal administration of DTx (23).

When CX3CR1-positive cells were eliminated during the phase of pathological angiogenesis at P13 (Fig. 3B and C) slight trends to lower pathological neovascularization and to increase vascular regeneration at P17 were observed (Fig. 3D). In contrast, when CX3CR1-positive cells were removed at P16 toward peak

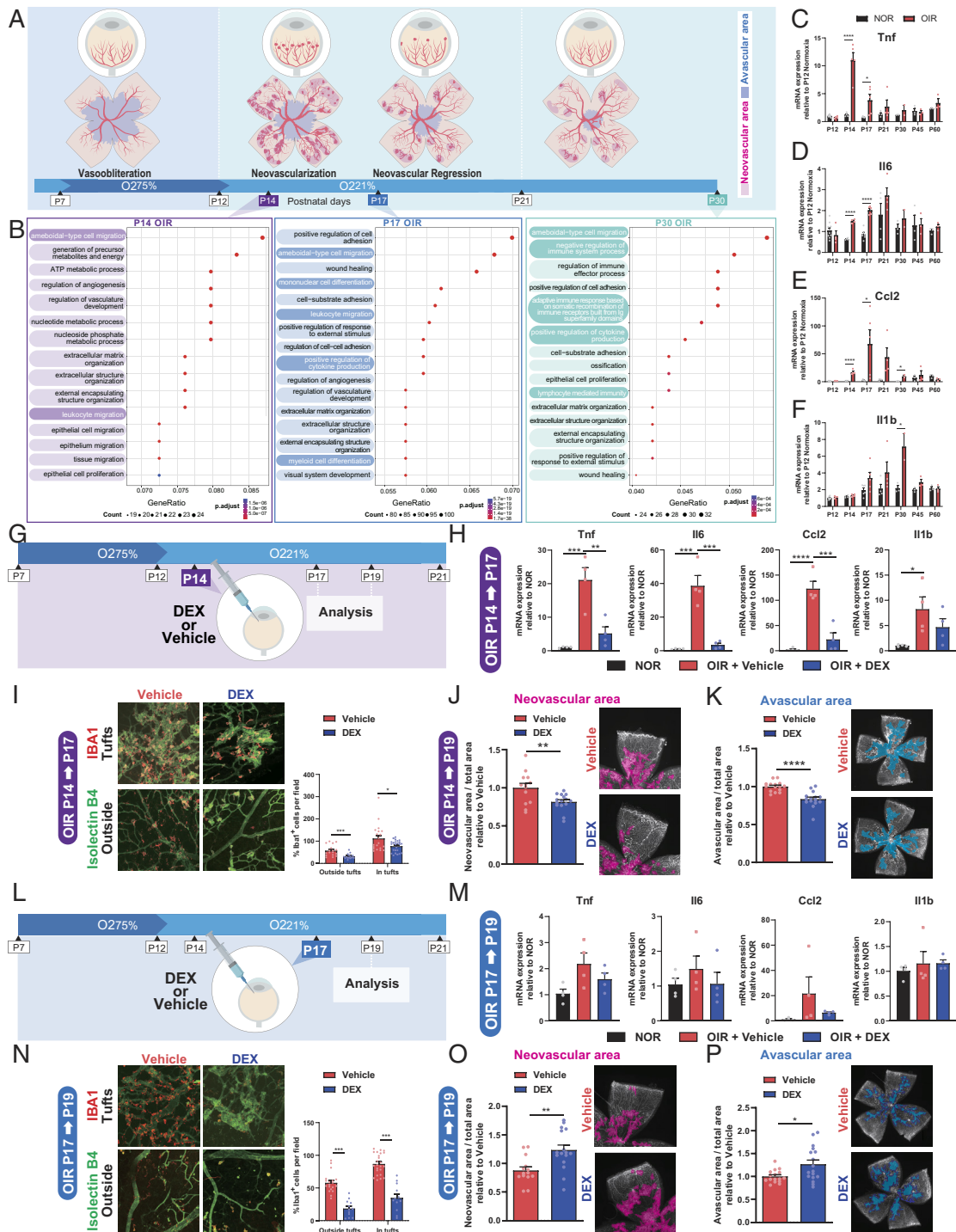


Fig. 1. Intravitreal dexamethasone treatment suppresses pathological neovascularization in early stages but prevents reparative vascular remodeling in later stages of disease. (A) Schematic representation of the mouse model of OIR and the distinct phases of the pathological vascularization (vaso-obliteration from P7 to P12, neovascularization from P12 to P17, and neovascular regression from P17). (B) Dot plots of the top 15 enriched Gene Ontology (GO) terms related to the biological processes for bulk RNA-seq from OIR and normoxic mouse retinas at P14, P17, and P30 (N = 2 to 3 mice per condition). The size of the dots represents the number of genes in the significant DE gene list associated with the GO term, and the color of the dots represents the *P*-adjusted values. Inflammation-related GO terms are highlighted. (C–F) mRNA expression of inflammation-related genes (C) *Tnf*, (D) *Il6*, (E) *Ccl2*, and (F) *Il1b* throughout the progression of OIR. Data are presented as fold change compared with P12 normoxic retinas (N = 3 to 10 depending on the group). Statistics were calculated comparing OIR versus normoxia for each given time point. (G) Schematic representation of intravitreal administration of dexamethasone (0.3 μ g) to P14 pups during OIR. (H) mRNA expression of *Tnf*, *Il6*, *Ccl2*, and *Il1b* (N = 4 per condition) in P17 retinas of OIR treated with or without dexamethasone (OIR + DEX, OIR + Vehicle, respectively) relative to normoxia. (I) IBA1⁺ phagocytes colocalized with isolectin-B4⁺ ECs were found in P17 flatmounts of OIR treated with or without dexamethasone (DEX and Vehicle, respectively) in neovascular tuft areas and outside tuft areas (N = 16 to 24 depending on the group). (J and K) Neovascular area (J) and avascular area (K) as assessed at P19 flatmounts of OIR treated with or without dexamethasone (N = 13 to 15 depending on the group). (L) Schematic representation of intravitreal administration of dexamethasone (0.3 μ g) to P17 pups during OIR. (M) mRNA expression of *Tnf*, *Il6*, *Ccl2*, and *Il1b* (N = 4 per condition) in P19 retinas of OIR treated with or without dexamethasone (OIR + DEX, OIR + Vehicle, respectively) relative to normoxia. (N) IBA1⁺ phagocytes colocalized with isolectin-B4⁺ ECs were found in P19 flatmounts of OIR treated with or without dexamethasone (DEX and Vehicle, respectively) in neovascular tuft areas and outside tuft areas (N = 12 to 24 depending on the group). (O and P) Neovascular area (O) and avascular area (P) as assessed at P19 flatmounts of OIR treated with or without dexamethasone (N = 14 to 17 depending on the group). Student's unpaired *t* test (C–F, J–K and N–P) and one-way ANOVA with Tukey's multiple-comparison test (H and M) were used; **P* < 0.05, ***P* < 0.01, ****P* < 0.001, and *****P* < 0.0001; error bars represent mean \pm SEM.

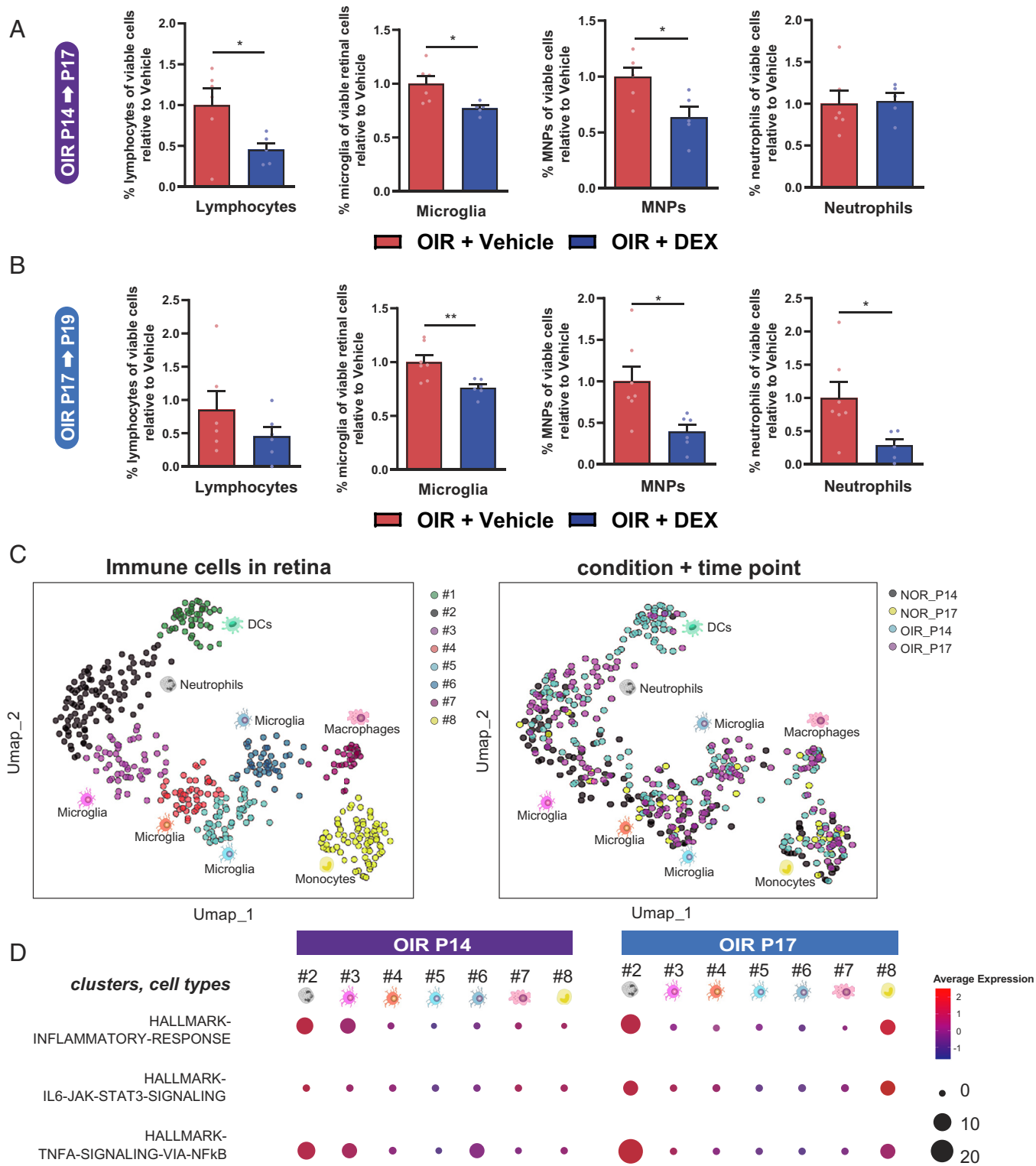


Fig. 2. Distinct populations of innate immune cells are elevated during neovascularization and vascular remodeling in ischemic retinopathy. (A and B) Flow cytometric analyses of OIR retinas treated with and without dexamethasone (OIR+DEX and OIR+Vehicle, respectively). Percentages of viable lymphocytes (CD45⁺/CD11b⁺/CD3ε⁺), microglia (CD45⁺/CD11b⁺/CX3CR1⁺), MNP (MNPs; CD45⁺/CD11b⁺/Ly6C^{int/high}/Ly6G^{low}), or neutrophils (CD45⁺/CD11b⁺/Ly6C^{int}/Ly6G^{high}) assessed at P17 (A) and P19 (B) by FACS (N = 5 to 7 depending on the group). (C) Uniform manifold approximation and projection (UMAP) plot for single-cell RNAseq of retinal immune cells from normoxic and OIR retinas at P14 and P17 (from two normoxic and three OIR sets of data). UMAP split according to immune cell populations (Left panel) and condition+timepoint (Right panel). Each dot represents one cell. (D) Dot plot representing results of Gene Set Variation Analysis (GSVA) for the inflammation-associated gene sets from Hallmark in each of the seven populations identified in (C) at P14 and P17 of OIR. Student's unpaired *t* test (A and B) were used; **P* < 0.05 and ***P* < 0.01; error bars represent mean ± SEM.

pathological angiogenesis and the onset of vascular remodeling, we observed a significant decrease in the area of pathological neovascularization and a significant increase in the extent of vascular

regeneration at P19 (Fig. 3E). This may have occurred as a consequence of lesser initial preretinal neovascularization or potentially implies CX3CR1-positive cells in impairing vascular repair in the later stage of OIR.

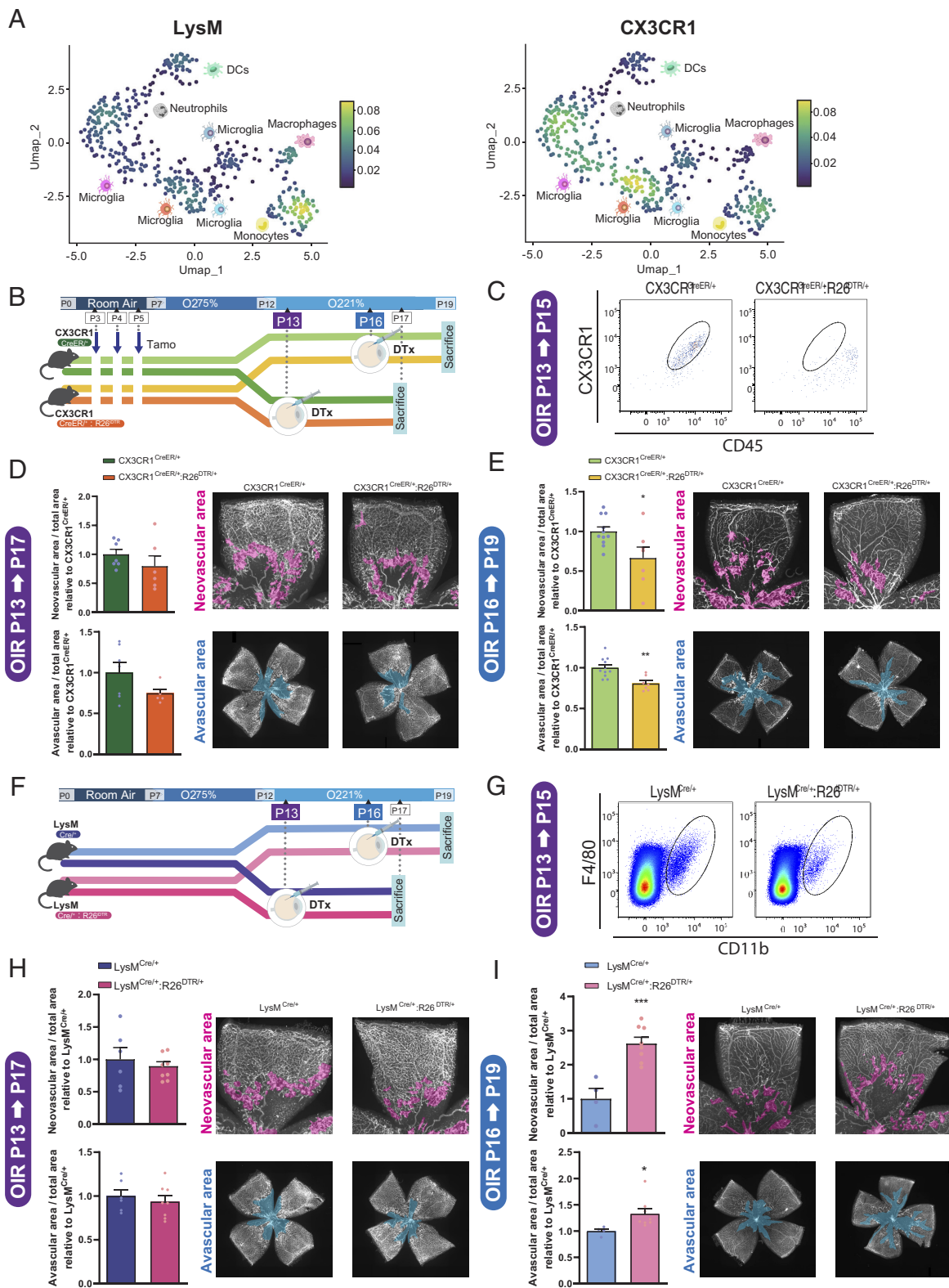


Fig. 3. LysM⁺ monocytes mediate vascular remodeling in later stages of OIR while CX3CR1-expressing cells contribute to angiogenesis. (A) UMAP visualization of the expression of two major myeloid marker genes *Lyz2* (Left panel) and *Cx3cr1* (Right panel) in retinal immune cells during OIR. (B) Time course of *Cx3cr1*^{CreER/+} and *Cx3cr1*^{CreER/+};R26^{DTR/+} OIR mice. For both *Cx3cr1*^{CreER/+} and *Cx3cr1*^{CreER/+};R26^{DTR/+} mice, tamoxifen (TAM) was administered daily between P3 and P5, and diphtheria toxin intravitreally (ivt) at either P13 or P16. (C) Representative FACS plots of CX3CR1⁺ microglia of retinas from *Cx3cr1*^{CreER/+} and *Cx3cr1*^{CreER/+};R26^{DTR/+} mice following intravitreal diphtheria toxin injection. (D) Neovascular area and avascular area as assessed at P17 flatmounts of OIR treated with or without dexamethasone at P13 (N = 6 or 7 depending on the group). (E) Neovascular area and avascular area as assessed at P19 flatmounts of OIR treated with or without dexamethasone at P16 (N = 7 or 11 depending on the group). (F) Time course of *LysM*^{Cre/+} and *LysM*^{Cre/+};R26^{DTR/+} OIR mice. For both *LysM*^{Cre/+} and *LysM*^{Cre/+};R26^{DTR/+} mice, TAM was administered daily between P3 and P5, and diphtheria toxin ivt at either P13 or P16. (G) Representative FACS plots of MNP of retinas from *LysM*^{Cre/+} and *LysM*^{Cre/+};R26^{DTR/+} mice following intravitreal diphtheria toxin injection. (H) Neovascular area and avascular area as assessed at P17 flatmounts of OIR treated with or without dexamethasone at P13 (N = 6 or 8 depending on the group). (I) Neovascular area and avascular area as assessed at P19 flatmounts of OIR treated with or without dexamethasone at P16 (N = 4 or 8 depending on the group). Student's unpaired *t* test (D, E, H and I) was used; **P* < 0.05, ***P* < 0.01, and ****P* < 0.001; error bars represent mean ± SEM.

Next, we eliminated LysM-positive cells during neovascularization (P13) and vascular remodeling (P16) with intravitreal administration of DTx (Fig. 3 F and G). Similar to CX3CR1-positive cells, depletion of LysM-positive cells at P13 led to a nonsignificant trend toward lower pathological neovascularization and vascular regeneration at P17 (Fig. 3H). However, removal of LysM-positive cells at P16 significantly compromised beneficial vascular remodeling and led to persistent pathological neovascularization and stalled vascular remodeling to a similar extent as what was observed with intravitreal dexamethasone (Fig. 3I). In agreement with scRNAseq data showing that neutrophils and monocytes up-regulate most robustly their inflammatory profiles prior to vascular regression (Fig. 2D), these results indicate that CX3CR1-positive and LysM-positive myeloid cells play distinct roles in vascular remodeling, with LysM-positive myeloid cells partaking in the clearance of pathological neovascularization and CX3CR1-expressing cells contributing to pathological angiogenesis.

Discussion

While nonresolving inflammation is typically associated with tissue damage and disease, the innate immune system's primary function is to fend off nonself pathogens and ensure tissue repair and homeostasis (24, 25). In this study, we put forward data highlighting that nonspecific inhibition of effectors of retinal immunity with corticosteroids can inhibit formation of pathological angiogenesis yet compromise intrinsic repair mechanisms that themselves remodel and eliminate diseased neovascularization. In addition, we provide evidence for a role for monocyte-like cells in driving beneficial vascular remodeling and microglia in mediating retinal neoangiogenesis.

Our data are in line with previous work demonstrating that subcutaneous injections of dexamethasone during the early stages of OIR (from P7 to P12) reduced retinal neovascularization at P17-20 (25), and current clinical data that demonstrate topical dexamethasone can decrease macular edema (26) and progression to severe Type II neovascular ROP (27). Yet, our data also highlight that the retinal immune system is critical for reparative vascular remodeling and nonspecifically dampening the inflammatory response at disease stages when vascular remodeling occurs can compromise tissue repair. Using mouse genetics, we demonstrate that the reparative properties of the innate immune system can be attributed LysM-expressing cells that are likely of monocytic origin. These findings agree with our previous work demonstrating enrichment of senescent endothelial cells in neovascular tufts (21, 28) with distinct secretomes that recruit effectors of innate immunity such as neutrophils to partake in clearing pathological vasculature (9). Interestingly, our data reveal that intravitreal dexamethasone reduces numbers of neutrophils and specifically in later stages of OIR associated with peak neovascularization. Given that neutrophils express LysM, their elimination from *LysM^{Cre/+};R26^{IDTR/+}* mice may contribute to impairing regression of pathological angiogenesis. Similarly, mice that are deficient in monocyte-chemoattractant protein-1 have delayed regression of neovascular tufts (3), further underscoring the importance of proper innate immune function in retinal vascular homeostasis.

Collectively, our data suggest that while initial triggers of pathological angiogenesis are governed by components of the innate immune system, impairing inflammation at the height of neovascularization in late stages of retinopathy may compromise beneficial vascular remodeling (9). Our findings support use of broad-spectrum anti-inflammatory drugs in treatment of active neovascular retinal disease yet suggest that their use may also impair endogenous repair mechanisms. This observation from animal

models may need to be considered in disease stages associated with elevated retinal neovascularization.

Methods

Mice. All animal studies were performed in compliance with the ARRIVE guidelines and the Association for Research in Vision and Ophthalmology Statement for the Use of Animals in Ophthalmic and Vision Research and were approved by the Animal Care Committee of the Maisonneuve-Rosemont Hospital Research Center in agreement with the guidelines established by the Canadian Council on Animal Care.

Animals were housed in the animal facility of the Hospital Maisonneuve-Rosemont Research Center under a 12 h light/dark cycle with ad libitum access to food and water unless indicated otherwise.

Homozygous *B6.129P2(C)-Cx3cr1^{tm2.1(cre/ERT2)Jung/J}* (referred to as *CX3CR1^{CreER}*) mice were crossed in-house with homozygous *C57BL/6-Gt(ROSA)26Sor^{tm1(HBEGF)Awai/J}* (referred to as *R26^{IDTR}*) mice to obtain heterozygous *CX3CR1^{CreER/+};R26^{IDTR/+}* mice.

Homozygous *B6.129P2-Lyz2^{tm1(cre)lfo/J}* (referred to as *LysMcre*) mice were crossed with homozygous *C57BL/6-Gt(ROSA)26Sor^{tm1(HBEGF)Awai/J}* (referred to as *R26^{IDTR}*) mice to obtain heterozygous or *LysM^{Cre/+};R26^{IDTR/+}* mice.

OIR Mouse Model. OIR was carried out as described previously (29). In brief, mouse pups (*C57BL/6J*, *CX3CR1^{CreER/+};R26^{IDTR/+}* or *LysM^{Cre/+};R26^{IDTR/+}* mice) and their corresponding fostering mothers (CD1 female) were exposed to 75% O₂ from P7 to P12 and returned to room air afterward. This model resembles aggressive neovascular features as in human ocular neovascular diseases such as proliferative DR (19, 30). Upon return to room air, hypoxia-driven epiretinal neovascularization develops from P14 onward (31).

Myeloid Cell Depletion. Microglia depletion was performed using *CX3CR1^{CreER/+};R26^{IDTR/+}* in which the activation of Cre recombinase (under the control of the *Cx3cr1* promoter) can be induced by TAM treatment and leads to surface expression of DTR on CX3CR1-expressing cells. At P3, P4, and P5, mice were subjected to daily intraperitoneal injections with TAM diluted in corn oil (0.05 mg per mouse per day) for three consecutive days.

To deplete *CX3CR1^{CreER/+};R26^{IDTR/+}* mice, diphtheria toxin was administered ivt (25 ng/1 μ L saline per eye) at P13 or P16. Depletion of *LysM^{Cre/+};R26^{IDTR/+}* mice was achieved similarly at P13 and P16.

Gene Set Enrichment Analysis From Mouse Retina RNA-Seq. GSEA was conducted using GSEA v4.0.1 software provided by Broad Institute of Massachusetts Institute of Technology and Harvard University. We used GSEA to validate correlation between molecular signatures in phenotypes of interest. Enrichment analysis was conducted on preranked lists based on shrunken log₂ fold changes from DESeq2 lfcShrink option. Default parameters were changed as follows: Gene sets of interest were found in a catalog of functional annotated gene sets from MSigDB; phenotype label was defined as "OIR" versus "Normoxia"; gene sets smaller than 15 and larger than 500 were excluded from the analysis; statistic used to score hits was defined as "weighted p1".

Bulk RNA-Seq Analysis. Bulk RNA-seq data were described in refs. 20, 21. edgeR package in R was used to identify the differentially expressed genes in OIR compared to normoxia at each time point, with an FDR threshold of 0.05. The analysis was performed in genes expressed at >1 count per million in two or more samples, and generalized linear models were used to compare gene expression data. GO analysis was performed using significantly up- or down-regulated genes and the enrichGO function from the clusterProfiler package with biological process ontologies, and top 20 genes ordered by gene ratio were plotted. Two or three biological replicates were performed (n = 2 normoxia and n = 2 OIR at P14, n = 3 normoxia and n = 3 OIR at P17, and n = 3 normoxia and n = 3 OIR at P30).

Droplet-Based Single-Cell RNA Sequencing Analysis. Unique molecular identifier (UMI) counts for normoxic and OIR retina scRNA-Seq replicates were merged into one single Digital Gene Expression (DGE) matrix and processed using the Seurat package (Spatial reconstruction of single-cell gene expression data). Cells expressing less than 100 genes and more than 10% of mitochondrial genes were filtered out. Single-cell transcriptomes were normalized by dividing by the total

number of UMIs per cell, then multiplying by 10,000. All calculations and data were then performed in log space [i.e., $\ln(\text{transcripts-per-10,000} + 1)$]. After aligning whole and rod-depleted datasets using canonical correlation analysis on the most variable genes in the DGE matrix, PCA identified 20 significant PC which served as input for dimensionality reduction and embedding into 2-dimensional space. To identify putative cell types in the embedded space, we used a density clustering approach and computed average gene expression for each of the identified cluster based on Euclidean distances. We then compared each of the different clusters to identify marker genes that were significantly enriched for each cluster. Transcriptomic differences between normoxic and OIR cell types were statistically compared using a negative binomial model and analyzed using visualization tools including RidgePlot and UMAP plot from the Seurat R Package. Single-cell gene expression profiles from each separate cell type identified by scRNA-Seq were further analyzed using GSVA. Two technical replicates were performed for P14 and P17.

Intravitreal Injections. Pups were injected ivt at P14 using a Hamilton syringe (10 μL) with a glass capillary coupled onto it. Each treated pup had both eyes injected with either 1 μL dexamethasone (0.3 mg/mL) or 1 μL of appropriate vehicle control. Animals were evaluated at different time points depending on the experiment.

Transcription Analysis by qPCR. RNA extraction was performed with snap-frozen mouse retinas using TRIzol reagent (Cat# 15596026; Invitrogen) and digested with DNase I (Sigma Aldrich; Cat# D4527) following manufacturer instructions to avoid genomic DNA amplification. Total RNA was reverse transcribed using a 5 \times All-In-One RT MasterMix (Cat# G590; Applied Biological Materials Inc.) according to the manufacturer's instructions. Gene expression was analyzed using Bright Green2 \times qPCR Master Mix-Low Rox in an Applied Biosystems 7,500 Real-Time PCR System (Thermo Fisher Scientific, Waltham, MA). Primer sequences used in this study are listed in *SI Appendix, Table S1*. Analysis of expression was followed using the $\Delta\Delta\text{CT}$ method. *Actb* expression was used as the reference housekeeping gene. Statistical analysis was performed on $\Delta\Delta\text{CT}$ values, and data were represented as the expression of the target genes normalized to *Actb* (folds of increase).

Retinal Immunohistochemistry. Enucleated eyes were fixed in PFA 4% for 1 h at room temperature and washed with PBS. The retina was microdissected and incubated in a blocking solution containing 3% of bovine serum albumin (BSA) for 1 h. Antibodies including fluorescence-labeled ISOLECTIN-B₄ (Cat# FL-1101, Vector Labs) and Cleaved Caspase-3 (Cat# 9661S, Cell Signaling Technologies) were diluted using the same solution and applied on the tissue overnight at 4 °C. After washes with PBS, species-appropriate fluorescence-conjugated secondary antibodies were applied for 1 h at room temperature. Samples were counter-stained with DAPI, mounted, and imaged using an Olympus FV1000 confocal microscope (Olympus Canada, Richmond Hill, ON, Canada).*

Analysis of Retinal Vasculature. Enucleated eyes were fixed in PFA 4% for 1 h at RT. Retinas were carefully dissected and incubated overnight at 4 °C with fluorescence-labeled ISOLECTIN-B₄ (IB₄) in PBS. After mounting, retinas were imaged using a Zeiss AxioObserver.Z1 microscope (Zeiss, Jena, Germany). To determine the extent of the avascular area or neovascularization area, images were processed using ImageJ (U. S. NIH, Bethesda, MD) and analyzed by the

SWIFT-neovascularization method as described previously (31). Results are expressed normalized to control.

Fluorescence-Activated Cell Sorting (FACS) on Retinas and RPE-Choroid-Sclera Complexes. Retinas and RPE-choroid-sclera complexes were cut into small pieces and homogenized in a solution of 750U/mL DNase I (Cat# D4527, Sigma-Aldrich) and 0.5 mg/mL of collagenase D (Cat# 1108886001, Roche) for 20 min at 37 °C. Homogenates were filtered through a 70 μm cell strainer, counted, and resuspended in PBS + 3% FBS. Viability of the cells was checked by 7-ADD (Cat# 420404; BioLegend) staining for 20 min at room temperature. After incubation with LEAF purified anti-mouse CD16/32 (Cat# 101310; BioLegend) for 10 min at 4°C to block FC receptors, cells were incubated for 25 min at 4 °C with the following antibodies: BV711 anti-mouse/human CD11b (Cat# 101242; BioLegend), PE anti-mouse CX3CR1 (Cat# FAB5825P; R&D), APC anti-mouse CD45.2 (Cat# 109814; BioLegend), APC/Cy7 anti-mouse Ly-6G (Cat# 127624; BioLegend), and PE/Cy7 anti-mouse F4/80 (Cat# 123114; BioLegend), or BV785 anti-mouse CD45.2 (Cat# 109839; BioLegend), FITC anti-mouse CD31 (Cat# 102506; BioLegend), and APC Annexin-V (Cat# 640919; BioLegend). FACS was performed on a BD LSR Fortessa™ \times -20 cell analyzer, and data were analyzed using FlowJo software (Version 10.2; FlowJo, Ashland, OR).

Statistical Analyses. Data are expressed as mean \pm SEM, unless indicated otherwise. Multiple Student's *t* tests, 2-tailed Student's *t* test, or ANOVA *t* test were used to compare two or more than two groups, respectively. Statistical significance was considered when $P < 0.05$ and noted as * $P < 0.05$, ** $P < 0.01$, *** $P < 0.001$, and **** $P < 0.0001$. All experimental Ns are indicated in the figure legends.

Data, Materials, and Software Availability. RNAseq and Single-cell RNA-seq data are deposited in NCBI's Gene Expression Omnibus and are accessible through GEO Accession No: [GSE158799](https://www.ncbi.nlm.nih.gov/geo/query/acc.cgi?acc=GSE158799) and [GSE150703](https://www.ncbi.nlm.nih.gov/geo/query/acc.cgi?acc=GSE150703). They were previously published in: (20, 21)

ACKNOWLEDGMENTS. We thank Vera Guber for the management of the mouse colony and the research assistants at the animal facilities. Masayuki H. holds the Banting Fellowship from the CIHR and Fellowship from Japan Society for the Promotion of Science. P.S. holds the Fonds de Recherche en Ophtalmologie de l'Université de Montréal Endowed Chair and Canada Research Chair in Retinal Cell Biology. This work was supported by the Canadian Institutes of Health Research (Foundation grant #353770), The Alcon Research Institute Senior Investigator Award, and The Heart and Stroke Foundation of Canada (G-16-00014658), BrightFocus Foundation (M20220151), and La Fondation Courtois. Additional support was provided by the *Fonds de Recherche en Ophtalmologie de l'Université de Montréal* (FROUM), the *Réseau en Recherche en Santé de la Vision* (RRSV), and the FRQ-S/RRSV-funded Single-Cell Academy.

Author affiliations: *Departments of Ophthalmology, Maisonneuve-Rosemont Hospital Research Centre, University of Montreal, Montreal, QC H1T 2M4, Canada; ^bDepartment of Biochemistry and Molecular Medicine, Maisonneuve-Rosemont Hospital Research Centre, University of Montreal, Montreal, QC H1T 2M4, Canada; ^cDepartments of Pediatrics, Ophthalmology, and Pharmacology, Centre Hospitalier, Universitaire Ste-Justine Research Center, Montréal, QC H3T 1C5, Canada; and ^dDepartment of Pathology and Tumour Biology, Graduate School of Medicine, Kyoto University, Kyoto 606-8315, Japan

1. C. Yu, C. Roubeix, F. Sennlaub, D. R. Saban, Microglia versus monocytes: Distinct roles in degenerative diseases of the retina. *Trends Neurosci.* **43**, 433–449 (2020).
2. K. Rashid, I. Akhtar-Schaefer, T. Langmann, Microglia in retinal degeneration. *Front. Immunol.* **10**, 1975 (2019).
3. M. H. Davies, A. J. Stempel, M. R. Powers, MCP-1 deficiency delays regression of pathologic retinal neovascularization in a model of ischemic retinopathy. *Invest. Ophthalmol. Vis. Sci.* **49**, 4195–4202 (2008).
4. A. Dejida *et al.*, Neuropilin-1 mediates myeloid cell chemoattraction and influences retinal neuroimmune crosstalk. *J. Clin. Invest.* **124**, 4807–4822 (2014).
5. V. Marchetti *et al.*, Differential macrophage polarization promotes tissue remodeling and repair in a model of ischemic retinopathy. *Sci Rep* **1**, 76 (2011).
6. J. Liu *et al.*, Myeloid cells expressing VEGF and arginase-1 following uptake of damaged retinal pigment epithelium suggests potential mechanism that drives the onset of choroidal angiogenesis in mice. *PLoS One* **8**, e72935 (2013).
7. F. Sennlaub *et al.*, CCR2(+) monocytes infiltrate atrophic lesions in age-related macular disease and mediate photoreceptor degeneration in experimental subretinal inflammation in Cx3cr1 deficient mice. *EMBO Mol. Med.* **5**, 1775–1793 (2013).
8. L. Zhao *et al.*, Microglial phagocytosis of living photoreceptors contributes to inherited retinal degeneration. *EMBO Mol. Med.* **7**, 1179–1197 (2015).
9. F. Binet *et al.*, Neutrophil extracellular traps target senescent vasculature for tissue remodeling in retinopathy. *Science* **369**, eaay5356 (2020).
10. T. Rhen, J. A. Cidlowski, Antiinflammatory action of glucocorticoids—new mechanisms for old drugs. *N. Engl. J. Med.* **353**, 1711–1723 (2005).
11. H. Schacke, W. D. Docke, K. Asadullah, Mechanisms involved in the side effects of glucocorticoids. *Pharmacol. Ther.* **96**, 23–43 (2002).
12. R. G. Ball, J. Lansbury, The treatment of a case of Addison's disease with the cortical hormone of Swingle and Pfiffner. *Can. Med. Assoc. J.* **24**, 695–697 (1931).
13. P. S. Hench, E. C. Kendall, C. H. Slocumb, H. F. Polley, The effect of a hormone of the adrenal cortex (17-hydroxy-11-dehydrocorticosterone: Compound E) and of pituitary adrenocortical hormone in arthritis: Preliminary report. *Ann. Rheum. Dis.* **8**, 97–104 (1949).
14. J. J. Bunim, R. L. Black, L. Lutwak, R. E. Peterson, G. D. Whedon, Studies on dexamethasone, a new synthetic steroid, in rheumatoid arthritis: A preliminary report; Adrenal cortical, metabolic and early clinical effects. *Arthritis Rheum.* **1**, 313–331 (1958).

15. Z. Sherif, U. Pleyer, Corticosteroids in ophthalmology: Past-present-future. *Ophthalmologica* **216**, 305-315 (2002).
16. S. A. Gaballa *et al.*, Corticosteroids in ophthalmology: Drug delivery innovations, pharmacology, clinical applications, and future perspectives. *Drug Deliv. Transl. Res.* **11**, 866-893 (2021).
17. A. W. Stitt *et al.*, The progress in understanding and treatment of diabetic retinopathy. *Prog. Retin. Eye Res.* **51**, 156-186 (2016).
18. R. Lee, T. Y. Wong, C. Sabanayagam, Epidemiology of diabetic retinopathy, diabetic macular edema and related vision loss. *Eye Vis. (Lond.)* **2**, 17 (2015).
19. L. E. Smith *et al.*, Oxygen-induced retinopathy in the mouse. *Invest. Ophthalmol. Vis. Sci.* **35**, 101-111 (1994).
20. G. Mawambo *et al.*, HIF1alpha-dependent hypoxia response in myeloid cells requires IRE1alpha. *J. Neuroinflam.* **20**, 145 (2023).
21. S. Crespo-Garcia *et al.*, Pathological angiogenesis in retinopathy engages cellular senescence and is amenable to therapeutic elimination via BCL-xL inhibition. *Cell Metab.* **33**, 818-832.e817 (2021).
22. I. M. Gan, L. C. Ugahary, J. T. van Dissel, J. C. van Meurs, Effect of intravitreal dexamethasone on vitreous vancomycin concentrations in patients with suspected postoperative bacterial endophthalmitis. *Graefes Arch. Clin. Exp. Ophthalmol.* **243**, 1186-1189 (2005).
23. M. Hata *et al.*, Past history of obesity triggers persistent epigenetic changes in innate immunity and exacerbates neuroinflammation. *Science* **379**, 45-62 (2023).
24. A. Lampron, A. Elali, S. Rivest, Innate immunity in the CNS: Redefining the relationship between the CNS and its environment. *Neuron* **78**, 214-232 (2013).
25. M. D. Nguyen, J. P. Julien, S. Rivest, Innate immunity: The missing link in neuroprotection and neurodegeneration? *Nat. Rev. Neurosci.* **3**, 216-227 (2002).
26. *Oculis* (2023).
27. H. M. Ohnell, S. Andreasson, L. Granse, Dexamethasone eye drops for the treatment of retinopathy of prematurity. *Ophthalmol. Retina* **6**, 181-182 (2022).
28. M. Oubaha *et al.*, Senescence-associated secretory phenotype contributes to pathological angiogenesis in retinopathy. *Sci. Transl. Med.* **8**, 362ra144 (2016).
29. K. Miloudi *et al.*, Assessment of vascular regeneration in the CNS using the mouse retina. *J. Vis. Exp.* **23**, e51351 (2014).
30. A. Stahl *et al.*, The mouse retina as an angiogenesis model. *Invest. Ophthalmol. Vis. Sci.* **51**, 2813-2826 (2010).
31. A. Stahl *et al.*, Computer-aided quantification of retinal neovascularization. *Angiogenesis* **12**, 297-301 (2009).